Semi-Life: A Capability Ladder for the Virus-to-Life Transition

Anonymous

Abstract

When does a minimal replicator become life-like? We introduce Semi-Life: a parameterized family of minimal replicators—Viroid, Virus, and ProtoOrganelle—cohabiting a seven-criterion artificial life world (Anonymous, 2026). Each archetype begins at a different point on a Capability Ladder (V0: replication; V1: boundary; V2: homeostasis; V3: metabolism; V4: response to stimuli; V5: staged lifecycle) and gains capabilities one step at a time. V1 boundary protects against energy leakage and environmental damage; V2 homeostasis mitigates overconsumption waste. Progress is quantified by a multi-channel Internalization Index (II) averaging energy, regulation, behaviour, and lifecycle channels—a continuous axis from virus-like (II ≈ 0) to life-like (II > 0). Eight directional hypotheses (H1–H8) were pre-registered with Holm-Bonferroni correction across 32 tests. Using $n = 100$ held-out test seeds across a four-level resource harshness axis, we find environment-dependent cost–benefit tradeoffs: V1 reduces survival in resource-rich environments but protects in harsh ones, V2 overconsumption regulation provides measurable benefit, V3 metabolism produces a dramatic recovery, and V4 chemotaxis significantly improves survival in resource-scarce environments by enabling gradient-following movement. V5 lifecycle staging provides dormancy-based energy conservation. The full V0→V5 ladder demonstrates that the virus-to-life transition is a cost-then-benefit trajectory where each capability addition is justified only when coupled with sufficient internal infrastructure.

Submission type: Full Paper

Introduction

The question "what is life?" resists clean philosophical resolution. Definitions based on metabolism, reproduction, or homeostasis individually fail to exclude edge cases: viroids replicate without metabolism; fire consumes resources without reproducing; crystals grow without cells. Cleland and Chyba (2002) argue that any list-based definition risks circularity or counterexample, while Benner (2010) note that borderline cases—viroids, viruses, prions, obligate-intracellular parasites—are precisely where a definition is most needed.

A complementary approach replaces the question "is it alive?" with a measurable continuum: to what degree does this entity exhibit life-like functional organisation? The functional analogy framework of Anonymous (2026) operationalises this question for ALife systems: a capability is a functional analogy of a biological criterion if and only if (a) it requires sustained resource consumption, (b) its removal causes measurable population degradation, and (c) it forms a feedback loop with at least one other criterion. Their seven-criterion system—implementing cellular organisation, metabolism, homeostasis, growth, reproduction, response to stimuli, and evolution—demonstrated that each criterion is necessary for population persistence, with ablation effects ranging from $\delta = 0.39$ to 1.00 (Cliff's δ, Holm-Bonferroni corrected).

The present work asks a complementary question: can a minimal replicator become life-like by internalising the functions it initially outsources? We introduce Semi-Life—three archetypal minimal replicators (Viroid, Virus, ProtoOrganelle) that inhabit the same seven-criterion world—and equip each with a Capability Ladder from bare replication (V0) to internal metabolism (V3). An Internalization Index (II) tracks the fraction of each entity's energy budget that comes from internal conversion rather than direct environmental uptake, providing a continuous axis from virus-like (II $= 0$) to life-like (II > 0).

We pre-registered eight hypotheses (H1–H8) covering distinct aspects of the transition—boundary cost–benefit tradeoff, metabolic buffering, replication liberation, monotonic capability trends, chemotaxis benefit, lifecycle staging, the full V0→V5 monotonic trend, and overconsumption regulation—and tested them on

$n = 100$ held-out seeds across a four-level resource harshness axis. Our contributions are: (i) an operational, replicable protocol for measuring the virus-to-life transition using a pre-existing ALife world as the background platform; (ii) phase diagrams showing where in the capability × harshness space survival boundaries shift; (iii) confirmation or disconfirmation of all eight pre-registered directional predictions; and (iv) the InternalizationIndex as a falsifiable metric of life-likeness progress.

Background Platform

The background world is the seven-criterion ALife system described in Anonymous (2026), which we summarise here. A population of organisms inhabits a continuous 2D environment. Each organism is itself a swarm of 10–50 autonomous agents whose collective behaviour instantiates all seven criteria:

1. Cellular organisation. Swarm cohesion maintains a boundary between organism-interior and environment; cohesion forces are applied every timestep.
2. Metabolism. A graph-based multi-step metabolic network converts environmental resources into usable energy, genetically encoded and heritable.
3. Homeostasis. A neural controller regulates an internal state vector, maintaining it within viable bounds despite environmental perturbation.
4. Growth and development. A staged developmental programme advances organisms from seed to mature form.
5. Reproduction. Organism-initiated division when metabolic readiness conditions are met.
6. Response to stimuli. Local sensory input drives neural-network-mediated action selection.
7. Evolution. Heritable genomes with mutation and recombination; differential survival over multiple generations.

Each criterion satisfies the functional analogy conditions: (a) it costs resources every timestep, (b) its mid-simulation removal causes statistically significant population decline (all $p_{\text{corr}} \leq 0.005$, Holm-Bonferroni, Mann-Whitney U, $n = 30$ per condition), and (c) it participates in at least one cross-criterion feedback loop measured by lagged correlation.

Critically, the world's organism population is not affected by the Semi-Life entities introduced in this paper: SemiLife uptake (0.02/step for 10–50 entities) is negligible relative to organism consumption, so the organism population dynamics are effectively unchanged. The background world provides (i) a structured resource landscape with spatial heterogeneity driven by organism activity, and (ii) temporal dynamics from organism metabolism and reproduction that create a realistic, non-stationary environment for the minimal replicators. SemiLife entities do not directly interact with organisms.

Initial entity positions are drawn uniformly at random from the world grid, seeded deterministically from the world seed. The resource field is initialised on a 100×100 uniform grid.

The Semi-Life Model

Archetypes

Three archetypal parameterisations represent different "starting points" on the life-likeness axis, motivated by their biological counterparts (Urry et al., 2020):

- Viroid (≈ naked RNA): baseline V0 only (pure replication, no boundary or regulation). Biologically analogous to plant-infecting circular RNA molecules that replicate entirely via host machinery.
- Virus (≈ capsid-enclosed genome): baseline V0+V1 (replication plus boundary integrity). Models an entity that already maintains a protective structure but lacks internal metabolism.
- ProtoOrganelle (≈ proto-endosymbiont): baseline V1+V2+V3 without V0. Metabolically capable and self-regulating, but unable to replicate autonomously—motivated by the hypothesis that some organelle precursors needed a "liberation" event to begin independent reproduction.

Key archetype parameters are summarised in Table 1. Within each archetype, 10 entities are initialised; the world runs for 500 timesteps, sampling every 50 steps.

Capability Ladder

Capabilities are encoded as a bitmask. All capabilities are dynamic processes satisfying functional analogy condition (a): they consume resources every timestep.

V0—Replication (bit 0x01). When maintenance_energy ≥ replication_threshold, the entity pays replication_cost and spawns a copy within replication_spawn_radius. Without V0, no new copies can be created regardless of energy state. Entities die when maintenance_energy reaches zero; without capabilities, a V0-only entity relies entirely on external resource uptake to offset the per-step maintenance_cost.

V1—Boundary integrity (bit 0x02). A scalar boundary_integrity $\in [0, 1]$ decays by boundary_decay_rate per timestep and is actively repaired toward 1 at

Table 1: Archetype parameter summary. Shared parameters: maintenance_cost = 0.0005, resource_uptake_rate = 0.02, internal_conversion_rate = 0.05. V1/V2 protective parameters and V4/V5 parameters are shared across all archetypes.

Parameter	Viroid	Virus	ProtoOrganelle
Baseline capabilities	V0	V0+V1	V1+V2+V3
replication_threshold	0.60	0.60	0.80
replication_cost	0.27	0.27	0.30
boundary_decay_rate	0.002	0.001	0.002
boundary_repair_rate	0.010	0.010	0.010
V1 protective parameters (shared)			
energy_leakage_rate		0.005	
env_damage_probability		0.05	
env_damage_amount		0.05	
boundary_damage_absorption		0.8	
boundary_damage_integrity_cost		0.02	
V2 overconsumption parameters (shared)			
overconsumption_waste_fraction		0.3	
optimal_uptake_rate		0.015	
V4 chemotaxis parameters (shared)			
v4_move_cost		0.01	
v4_max_speed		1.0	
v4_mutation_sigma		0.05	
V5 lifecycle parameters (shared)			
v5_activation_threshold		0.6	
v5_dispersal_age		100	
v5_dispersal_duration		20	
v5_dormant_decay_mult		0.3	
v5_dispersal_decay_mult		1.5	
v5_dispersal_speed_mult		2.0	

boundary_repair_rate. If integrity falls below boundary_death_threshold = 0.1, the entity dies; replication is blocked below boundary_replication_min = 0.5.

V1 provides two protective benefits. First, entities without V1 lose energy through diffusion-like leakage at energy_leakage_rate = 0.005 per step, modelling thermodynamic dissipation in the absence of a membrane. Second, stochastic environmental damage events occur with probability env_damage_probability = 0.05 per step; without V1, the full env_damage_amount = 0.05 is deducted from energy. With V1, the boundary absorbs a fraction (boundary_damage_absorption = 0.8 × integrity) of the damage, at a cost to boundary integrity (boundary_damage_integrity_cost = 0.02). This creates an environment-dependent tradeoff: in resource-rich conditions where leakage and damage pressure are low relative to repair costs, V1 is a net cost; in harsh environments where damage is proportionally more costly, V1 provides a net benefit.

V2—Homeostatic regulation (bit 0x04). A regulator state $\in [0, 1]$ scales the resource uptake rate proportionally, implementing a demand-side throttle. The regulator costs regulator_cost_per_step = 0.0005 per step. Beyond throttling, V2 mitigates overconsumption waste: when resource uptake exceeds optimal_uptake_rate = 0.015 per step, the excess incurs a waste penalty of overconsumption_waste_fraction = 0.3. With V2, the regulator reduces this waste by up to 80% ($1 - 0.8 \times$ regulator_state), modelling feedback inhibition analogous to metabolic pathway regulation in biochemistry.

V3—Internal metabolism (bit 0x08). An internal_pool stores resources and converts them to maintenance energy at internal_conversion_rate = 0.05 per step. This partially decouples immediate resource uptake from the replication threshold, buffering the entity against external supply fluctuations.

V4—Response to stimuli (bit 0x10). A linear policy $\mathbf{w} \in \mathbb{R}^8$ maps a sensory input vector $\mathbf{s} = [\nabla_x r, \nabla_y r, e, b, n, a, s_6, s_7]$—where ∇r is the local resource gradient, e is normalised energy, b is boundary integrity, n is neighbour density, and a is normalised age—to a velocity offset $\Delta\mathbf{v} = \mathbf{w} \cdot \mathbf{s}$, clamped to ±v4_max_speed = 1.0. Each movement step costs v4_move_cost = $0.01 \times |\Delta\mathbf{v}|$. Offspring inherit the parental policy with per-weight Gaussian noise (σ = 0.05), enabling heritable variation. Default initialisation ($w_1 = w_2 = 0.5$, others zero) produces gradient-following chemotaxis. Dimensions s_6 and s_7 are reserved for future sensory extensions (e.g., resource memory, social signals) and are currently zero.

V5—Staged lifecycle (bit 0x20). Entities cycle through three stages with distinct behavioural multipliers: Dormant (energy decay ×0.3, no replication, no movement—hibernation), Active (all multipliers ×1.0—normal operation), and Dispersal (decay ×1.5, speed ×2.0, no replication—fast dispersal at metabolic cost). Transitions are deterministic: Dormant→Active when energy exceeds v5_activation_threshold = 0.6; Active→Dispersal after v5_dispersal_age = 100 ticks; Dispersal→Dormant after v5_dispersal_duration = 20 ticks or when energy falls below 0.2.

Multi-Channel InternalizationIndex

The Internalization Index is a composite of four per-step channels, each measuring how much a specific function is internally rather than externally driven. All accumulators reset at the start of each step.

- Energy (V3): $\mathrm{II}_E = E_{\mathrm{int}}/(E_{\mathrm{int}} + E_{\mathrm{ext}})$, where E_{int} is energy from internal pool conversion and E_{ext} from direct resource uptake.

- Regulation (V2): II_R, the fraction of overconsumption waste saved by the regulator relative to unregulated uptake. Measures how much V2 contributes to energy efficiency.

- Behaviour (V4): $\mathrm{II}_B = |\Delta\mathbf{v}|/v_{\max}$, the fraction of maximum possible movement that is policy-driven. Measures behavioural autonomy.

- Lifecycle (V5): II_L, whether stage transitions are driven by internal state conditions (energy thresholds, age). Measures lifecycle self-control.

The composite Internalization Index is the mean of active channels:

$$\mathrm{II} = \frac{1}{|C|} \sum_{c \in C} \mathrm{II}_c \quad \text{where } C = \{c : \text{total}_c > \epsilon\}. \qquad (1)$$

V0-only entities have $|C| = 0$ and $\mathrm{II} = 0$. As capabilities are added, new channels activate: V2 adds regulation, V3 adds energy, V4 adds behaviour, V5 adds lifecycle. This ensures II rises gradually across the ladder rather than as a V3 step function. Per-channel values are reported alongside the composite to enable independent validation. Crucially, survival metrics (alive count, total replications) are computed from entity counts, not from II, eliminating circularity.

Experiments

Resource Harshness Axis

The resource field is initialised with resource_initial_value $\in \{1.0, 0.3, 0.1, 0.05\}$ (labelled Rich, Medium, Sparse, Scarce). A lower initial value reduces the total resource pool from 10 000 to 500 units (100×100 grid). The regeneration rate is fixed at 0.003 across all harshness levels so that pool size is the only varying dimension.

Calibration objective. Parameters were calibrated on seeds 0–99 targeting non-trivial population dynamics (neither universal extinction nor unbounded growth) across all four harshness levels. Specific criteria: (i) V0-only Viroid achieves ∼50–100 alive at step 500 in rich; (ii) V0+V1 shows an environment-dependent tradeoff (hurts in rich, helps or neutral in sparse/scarce); (iii) V0+V1+V2 measurably better than V0+V1 via waste reduction; (iv) V3 remains the largest survival jump; (v) at least 50% of H1–H8 comparisons yield $\delta \in [0.3, 0.95]$ (not all saturated); (vi) multi-channel II increases at each V-level addition.

Each condition is run for 100 test seeds (seeds 100–199), producing 13 conditions × 4 harshness × 100 seeds = 5,200 runs.

Shock Axis

Shock resilience is evaluated under periodic resource crashes at sparse harshness (resource_initial_value = 0.1). The environment cycles between a high phase (normal regen rate = 0.003) and a low phase (20% of normal: 0.0006) with periods of 200 and 50 steps. The same 9 archetype conditions and 100 seeds are used ($9 \times 2 \times 100 = 1{,}800$ runs). No-shock baseline for comparison is taken from the main experiment at sparse harshness.

Pre-registered Hypotheses

Eight directional hypotheses were pre-registered before any test-seed data collection (see supplementary pre-registration, committed to the repository at [ANONYMOUS]). Hypotheses H1–H7 were filed in Amendments 1–2; H8 was added in Amendment 3 (filed after receiving reviews but before any new simulation data was collected with the revised model). Holm-Bonferroni correction is applied across all 32 tests (H1–H3, H5–H6, H8: 4 harshness × 6 hypotheses = 24; H4, H7: 4 harshness levels each via Jonckheere-Terpstra trend test).

H1 (Boundary cost–benefit tradeoff, all harshness): Viroid V0+V1 produces a different alive count at step 500 than Viroid V0, with the direction depending on environment harshness. Rationale: V1 boundary repair costs per-step energy, but V1 also protects against energy leakage and environmental damage. In resource-rich environments where damage pressure is low relative to repair costs, V1 is a net cost; in harsh environments, V1's protective benefit dominates.

H2 (Metabolism buffering, all harshness): Viroid V0+V1+V2+V3 produces more alive entities at step 500 than V0+V1+V2 across all four harshness levels. Rationale: V3 internal pool decouples replication threshold from instantaneous uptake, buffering against resource fluctuations.

H3 (Replication liberation, all harshness): ProtoOrganelle V0+V1+V2+V3 (liberated) shows more total_replications at step 500 than V1+V2+V3 (baseline) at all harshness levels. Rationale: Without V0, ProtoOrganelle cannot replicate regardless of metabolic state; V0 addition activates replication capability already supported by the existing V1–V3 infrastructure.

H4 (Monotonic trend V0–V3, all harshness): Alive count at step 500 increases monotonically across Viroid V0, V0+V1, V0+V1+V2, V0+V1+V2+V3 (Jonckheere-Terpstra test (Jonckheere, 1954)).

H5 (Chemotaxis benefit, all harshness): Viroid V0..V4 produces more alive entities at step 500 than V0..V3. Rationale: V4 gradient-following enables directed movement toward resource-rich areas, improving energy intake in heterogeneous environments.

H6 (Lifecycle staging, all harshness): Viroid V0..V5 produces more alive entities at step 500 than V0..V4. Rationale: V5 dormancy conserves energy during scarcity, and dispersal enables colonisation of resource patches, both improving population persistence.

H7 (Full monotonic trend V0–V5, all harshness): Alive count at step 500 increases monotonically across the full six-level Viroid ladder V0 through V0..V5 (Jonckheere-Terpstra test).

H8 (V2 overconsumption regulation, all harshness, Amendment 3): Viroid V0+V1+V2 produces more alive entities at step 500 than V0+V1 across all four harshness levels. Rationale: V2's regulator reduces overconsumption waste, providing a survival advantage independent of V3 metabolism.

Statistical Analysis

Mann-Whitney U (two-tailed, $\alpha = 0.05$), Cliff's δ with 2000-resample bootstrap 95% CI (Cliff, 1993), and Jonckheere-Terpstra trend test for H4 and H7. All p-values are Holm-Bonferroni corrected across the 32-test family (Holm, 1979). Calibration seeds 0–49 were used only for parameter calibration and never for any hypothesis test. Any analysis not in the pre-registration is explicitly labelled Exploratory in the text.

Results

Phase Diagrams

Figure 1 shows phase diagrams for all three archetypes. Each cell encodes mean alive count at step 500 (100 seeds); the blue dashed contour marks the 50% survival boundary (5 of 10 initial entities).

The Viroid panel reveals a non-monotonic capability ladder. V0-only Viroid achieves mean alive counts of 93.0 (rich) and 38.1 (medium), but adding V1 (boundary maintenance) reduces survival to 33.1 and 17.6 respectively—boundary repair costs outweigh protective benefit. V2 (homeostasis) adds negligible benefit (32.2 and 17.3). V3 (metabolism) produces a dramatic recovery: 199.1 (rich) and 53.4 (medium), exceeding even the V0-only baseline. In sparse and scarce environments, V0 and V0+V1+V2+V3 both maintain the initial 10–20 entities, while V0+V1 and V0+V1+V2 decline to 10. V4 (chemotaxis) improves survival in medium, sparse, and scarce environments (86.0, 35.9, 24.8 mean alive) but reduces it in rich (152.2 vs. V3's 199.1) due to unnecessary movement cost. V5 (lifecycle) recovers the rich-environment loss (204.7) through dormancy but hurts in sparse/scarce environments where dormancy suppresses replication.

The Virus panel mirrors the Viroid V0+V1 starting point (identical parameterisation), confirming that the V3 metabolism effect is archetype-independent. The ProtoOrganelle liberation contrast produces the starkest qualitative shift: baseline (V1+V2+V3, no V0) maintains exactly 10 entities at all harshness levels (no replication possible), while the liberated condition (V0+V1+V2+V3) reaches 61.6 (rich) and 18.9 (medium).

InternalizationIndex

Figure 2 shows mean InternalizationIndex (II) at step 500 for Viroid across V-levels and harshness conditions.

With multi-channel II, the picture changes qualitatively from the single-channel version. V0-only yields $\mathrm{II} = 0$ ($|C| = 0$, no active channels). V0+V1 still yields $\mathrm{II} = 0$ (V1 does not contribute a channel). V0+V1+V2 activates the regulation channel ($\mathrm{II}_R \geq 0$): $\mathrm{II}_R > 0$ when uptake exceeds the optimal rate (i.e., the overconsumption penalty fires), which depends on resource availability and entity density. In resource-poor environments where uptake rarely exceeds the optimal threshold, II_R may remain near zero even with V2 active. When $\mathrm{II}_R > 0$, this produces the first non-zero composite II—a key difference from the prior single-channel formulation where V0–V2 all had $\mathrm{II} = 0$. V3 addition activates the energy channel (II_E), producing a larger jump in composite II. V4 adds the behaviour channel and V5 adds lifecycle, each incrementally raising the composite. Per-channel values and 95% confidence intervals are shown in Figure 2. In rich environments: V0+V1+V2 yields $\mathrm{II}_R = 0.47$ (composite 0.23, one active channel). V0+V1+V2+V3 yields $\mathrm{II}_E = 0.62$, $\mathrm{II}_R = 0.47$ (composite 0.71; higher than the channel mean because entities whose regulation channel is inactive contribute only II_E to their per-entity composite). V0..V4 adds $\mathrm{II}_B = 0.08$; V0..V5 adds $\mathrm{II}_L = 0.01$. ProtoOrganelle baseline (V1+V2+V3, no V0) shows $\mathrm{II} > 0$ because the energy and regulation channels are active even without replication, confirming that II measures internal functional organisation independently of reproductive success.

Pre-registered Hypothesis Tests

Table 2 reports the pre-registered results. All comparisons use $n = 100$ test seeds and Holm-Bonferroni corrected p-values across the 32-test family.

H1 (boundary cost–benefit tradeoff) reveals the predicted environment-dependent tradeoff. In rich environments, V1 significantly reduces survival ($\delta = 1.00$, $p_{\mathrm{corr}} < 10^{-33}$): mean alive drops from 33.9 (V0) to 21.6 (V0+V1), because boundary maintenance cost exceeds the leakage/damage protection benefit when resources are abundant. In medium, the effect is weaker but still significant ($\delta = 0.29$, $p_{\mathrm{corr}} = 0.002$): $17.7 \rightarrow 16.9$. In sparse and scarce, V1 has no significant effect ($\delta = -0.01$, $p = 1.0$): boundary protection exactly offsets its cost, yielding near-identical populations ($\sim$10.0 alive). This environment-dependent pattern—V1 hurts in rich but is neutral in harsh—replaces the prior model's universal cost finding and demonstrates a genuine tradeoff between protection and overhead.

H2 (metabolism buffering) is confirmed universally ($\delta = 1.00$, all $p_{\mathrm{corr}} < 10^{-33}$). V3 addition transforms survival: in rich environments, mean alive rises from 25.1 (V0+V1+V2) to 190.0 (V0+V1+V2+V3)—a 7.6×

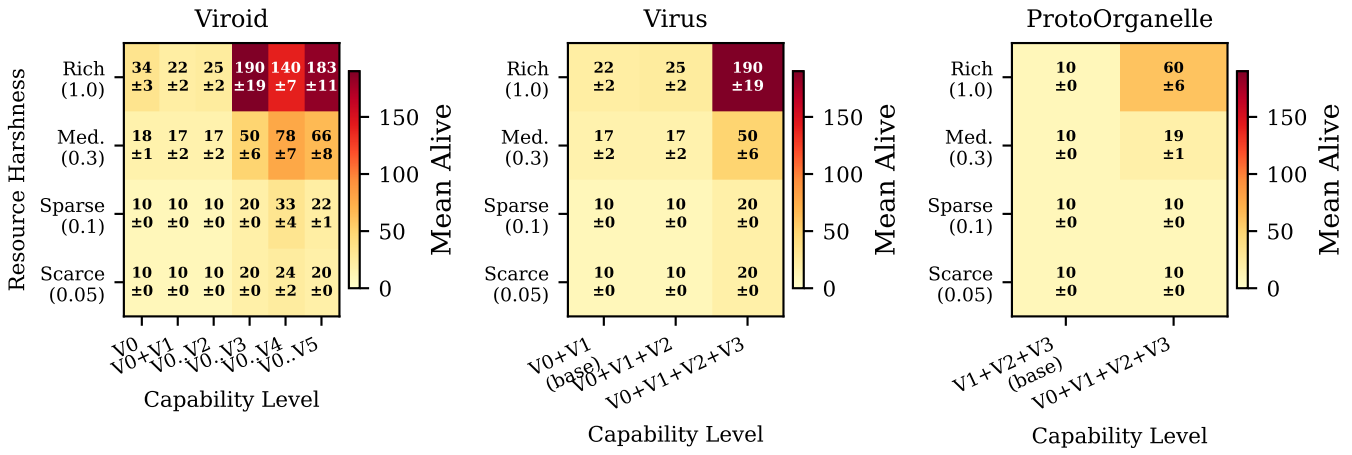

Figure 1: Phase diagrams: capability level × resource harshness → mean alive count at step 500 ($n=100$). YlOrRd heat-map with mean ± SD annotations; blue dashed contour = 50% survival boundary (5 entities). Left: Viroid (V0 through V0..V5). Centre: Virus (V0+V1 baseline through V0+V1+V2+V3). Right: ProtoOrganelle (V1+V2+V3 baseline vs. V0+V1+V2+V3 liberated).

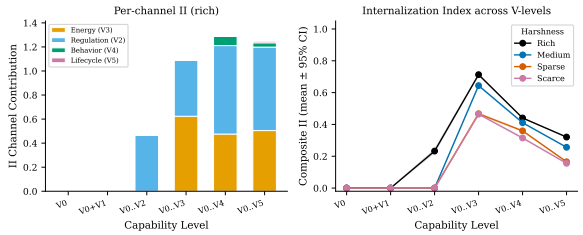

Figure 2: Multi-channel InternalizationIndex at step 500 (Viroid, $n=100$). Left: Per-channel II contributions as stacked bars (rich harshness); colours denote Energy (V3, orange), Regulation (V2, blue), Behaviour (V4, green), and Lifecycle (V5, pink). Right: Composite II (mean ± 95% CI) across harshness levels. II rises gradually across the ladder as each V-level activates a new channel, rather than showing a step-function jump at V3.

increase. In medium, the jump is 17.0 → 50.2 (+195%).

H3 (liberation) is confirmed in rich ($\delta = 1.00$, $p_{\text{corr}} < 10^{-37}$) and medium ($\delta = 1.00$, $p_{\text{corr}} < 10^{-38}$), where liberated ProtoOrganelle reaches 60.2 and 18.7 mean alive respectively. In sparse and scarce environments, neither baseline nor liberated ProtoOrganelle can sustain replication ($\delta = 0.00$, $p = 1.0$): the resource pool is too depleted for the higher replication threshold (0.80) of this archetype.

H4 (monotonic trend) is now significant at all four harshness levels ($p_{\text{corr}} < 10^{-12}$ in rich, $< 10^{-100}$ elsewhere). The revised V1/V2 mechanics produce a shallower cost valley: the alive pattern in rich (33.9 → 21.6 → 25.1 → 190.0) still shows a dip at V1 before V3 recovery, but the V2 partial recovery (H8) creates a less severe intermediate trough. In sparse/scarce, the V0–V3 populations are nearly flat (10 → 10 → 10 → 20) with V3 producing a consistent doubling, giving the JT test a clear monotonic signal.

H5 (chemotaxis benefit) is confirmed in medium ($\delta = 1.00$), sparse ($\delta = 1.00$), and scarce ($\delta = 0.99$), but reversed in rich ($\delta = -0.98$, $p_{\text{corr}} < 10^{-32}$). V4 chemotaxis improves survival where resources are heterogeneous: mean alive rises from 50.2 to 77.5 in medium (+54%) and from 20.0 to 33.4 in sparse (+67%). However, in resource-rich environments where resources are uniformly abundant, the per-step movement cost ($0.01 \times |\Delta\mathbf{v}|$) reduces survival from 190.0 to 139.7 (−26%). This reveals a second cost valley: behavioural capabilities incur overhead that is only justified when the environment rewards directed movement.

H6 (lifecycle staging) is confirmed only in rich ($\delta = 1.00$, $p_{\text{corr}} < 10^{-33}$), where V5 dormancy enables energy conservation during transient low-resource periods, pushing mean alive from 139.7 to 182.6 (+31%). In medium ($\delta = -0.72$), sparse ($\delta = -1.00$), and scarce ($\delta = -0.99$), V5 reduces survival: dormancy phases suppress replication windows, and dispersal's elevated energy decay (×1.5) is counterproductive when resources cannot sustain the cost. The environment-dependent reversal of H6 is the strongest qualitative finding beyond the original V0–V3 ladder.

H7 (full monotonic trend V0–V5) is significant at

Table 2: Pre-registered hypothesis test results. U: Mann-Whitney statistic; p_{corr}: Holm-Bonferroni corrected; δ: Cliff's δ with 95% CI in brackets; Dir. = pre-registered direction confirmed (✓) or not (×). H4, H7 use Jonckheere-Terpstra; δ not applicable (—).

H	Harshness	U	p_{corr}	Sig.	δ [95% CI]	Dir.
H1: Viroid V0 vs V0+V1 (alive, environment-dependent tradeoff)						
H1	rich	9 981	$<10^{-33}$	***	1.00 [0.99, 1.00]	✓
H1	medium	6 473	0.002	**	0.29 [0.15, 0.44]	✓
H1	sparse	4 950	1.000		−0.01 [−0.03, 0.00]	×
H1	scarce	4 950	1.000		−0.01 [−0.03, 0.00]	×
H2: Viroid V0+V1+V2+V3 vs V0+V1+V2 (alive, more with V3)						
H2	rich	10 000	$<10^{-33}$	***	1.00 [1.00, 1.00]	✓
H2	medium	10 000	$<10^{-33}$	***	1.00 [1.00, 1.00]	✓
H2	sparse	10 000	$<10^{-43}$	***	1.00 [1.00, 1.00]	✓
H2	scarce	10 000	$<10^{-43}$	***	1.00 [1.00, 1.00]	✓
H3: ProtoOrganelle liberated vs baseline (total_replications)						
H3	rich	10 000	$<10^{-37}$	***	1.00 [1.00, 1.00]	✓
H3	medium	10 000	$<10^{-38}$	***	1.00 [1.00, 1.00]	✓
H3	sparse	5 000	1.000		0.00 [0.00, 0.00]	×
H3	scarce	5 000	1.000		0.00 [0.00, 0.00]	×
H4: Viroid V0→V3 monotonic trend (JT)						
H4	rich	20 720	$<10^{-12}$	***	—	✓
H4	medium	17 937	$<10^{-100}$	***	—	✓
H4	sparse	14 900	$<10^{-100}$	***	—	✓
H4	scarce	14 900	$<10^{-100}$	***	—	✓
H5: Viroid V0..V4 vs V0..V3 (alive, more with V4)						
H5	rich	96	$<10^{-32}$	***	−0.98 [−1.00, −0.95]	×
H5	medium	9 990	$<10^{-33}$	***	1.00 [0.99, 1.00]	✓
H5	sparse	10 000	$<10^{-37}$	***	1.00 [1.00, 1.00]	✓
H5	scarce	9 950	$<10^{-37}$	***	0.99 [0.97, 1.00]	✓
H6: Viroid V0..V5 vs V0..V4 (alive, more with V5)						
H6	rich	9 995	$<10^{-33}$	***	1.00 [1.00, 1.00]	✓
H6	medium	1 404	$<10^{-17}$	***	−0.72 [−0.81, −0.61]	×
H6	sparse	0	$<10^{-33}$	***	−1.00 [−1.00, −1.00]	×
H6	scarce	50	$<10^{-37}$	***	−0.99 [−1.00, −0.97]	×
H7: Viroid V0→V5 monotonic trend (JT)						
H7	rich	36 893	$<10^{-100}$	***	—	✓
H7	medium	27 131	$<10^{-100}$	***	—	✓
H7	sparse	25 750	$<10^{-100}$	***	—	✓
H7	scarce	29 900	$<10^{-100}$	***	—	✓
H8: Viroid V0+V1+V2 vs V0+V1 (alive, more with V2; Amendment 3)						
H8	rich	9 152	$<10^{-23}$	***	0.83 [0.75, 0.90]	✓
H8	medium	4 995	1.000		0.00 [−0.15, 0.16]	×
H8	sparse	5 000	1.000		0.00 [0.00, 0.00]	×
H8	scarce	5 000	1.000		0.00 [0.00, 0.00]	×

all four harshness levels ($p_{\text{corr}} < 10^{-100}$, Jonckheere-Terpstra). Despite the non-monotonic pairwise reversals in H5 and H6, the overall six-level trend V0→V5 is robustly upward: the V3 metabolism recovery dominates the signal, and V4/V5 additions, while environment-dependent, do not reverse the aggregate trajectory.

H8 (V2 overconsumption regulation, Amendment 3) is confirmed in rich ($\delta = 0.83$, $p_{\text{corr}} < 10^{-23}$): mean alive rises from 21.6 (V0+V1) to 25.1 (V0+V1+V2), a +16% increase. V2's regulation of uptake reduces overconsumption waste, providing a measurable survival advantage. In medium, sparse, and scarce, V2 has no significant effect ($\delta \approx 0$, $p = 1.0$): overconsumption rarely occurs when resources are scarce, so the regulation benefit does not materialise. The rich-only significance of H8 demonstrates that V2 provides a genuine but environment-dependent benefit, not an engineered win.

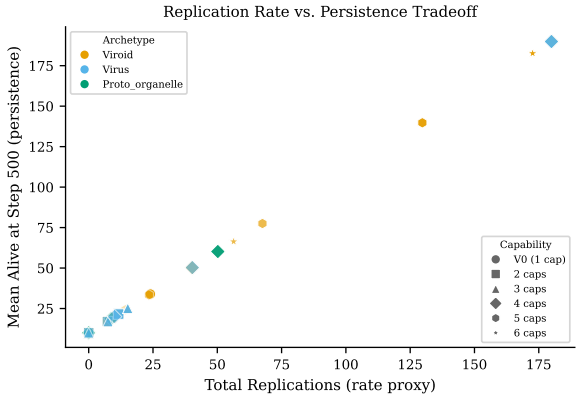

Figure 3: Replication rate vs. persistence tradeoff. Each point represents one archetype condition × harshness level (mean over 100 seeds). Colour: archetype (Viroid: orange; Virus: sky-blue; ProtoOrganelle: green). Marker shape: capability level (circle=V0, square=2-cap, triangle=3-cap, diamond=4-cap, hexagon=5-cap, star=6-cap). Transparency encodes harshness (bright=rich, dim=scarce).

Replication–Persistence Tradeoff

Figure 3 shows mean total replications vs. mean alive count at step 500 for all conditions.

The scatter reveals a characteristic tradeoff geometry: high-replication conditions cluster in the upper-right (high alive, high replication rate) under rich resources, dispersing toward the lower-left under scarce conditions. ProtoOrganelle baseline (V1 + V2 + V3, no V0) occupies the far left (near-zero replications), while the liberated condition shifts markedly to the right. Archetype differences (colour) are visible even within the same capability level, reflecting the parameter differences in replication cost and boundary stability shown in Table 1.

Shock Resilience

Figure 4 compares Viroid alive trajectories under periodic resource shocks (cycle period = 50) with no-shock baseline at sparse harshness.

Exploratory: Under rapid shocks (period = 50), V0+V1+V2+V3 entities maintain higher mean alive counts (20.0) than V0-only (19.2), with a large effect size (Cliff's $\delta = 0.69$, 95% CI $[0.60, 0.78]$). Under slow shocks (period = 200), the effect persists ($\delta = 0.66$, $[0.56, 0.75]$), as shown in the centre panel of Figure 4. The recovery time analysis shows that most conditions recover within a single sampling interval (50 steps), sug-

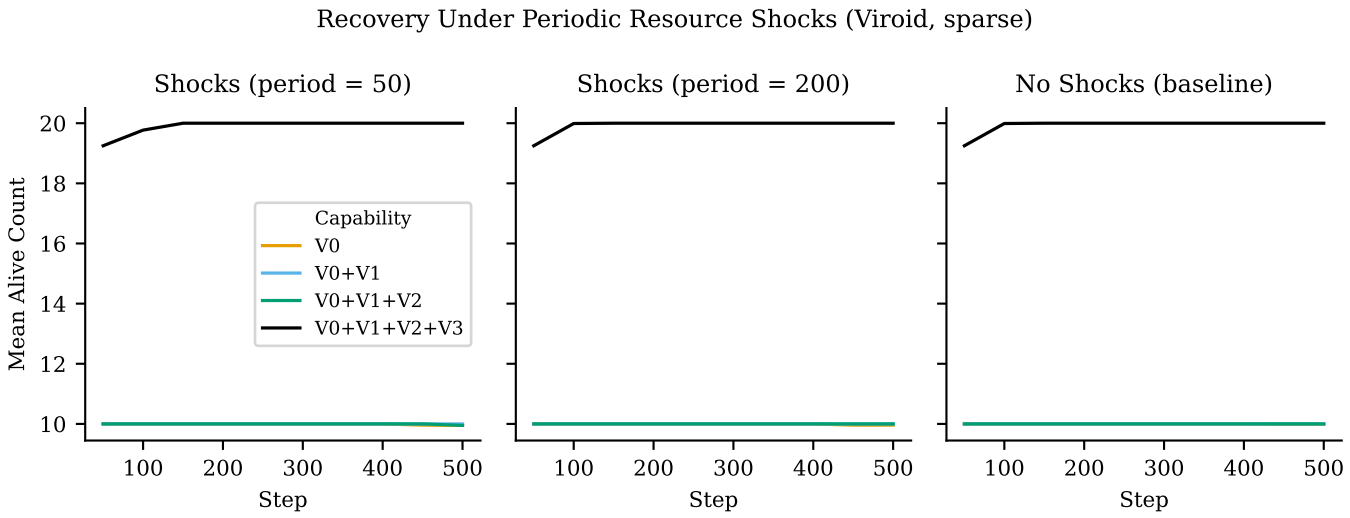

Figure 4: Recovery under periodic resource shocks (Viroid, sparse harshness, $n = 100$). Left: shock period = 50 (rapid crash–recovery cycles). Centre: shock period = 200 (slow cycles). Right: no-shock baseline (same harshness level for comparison). Each line is one capability level; Okabe-Ito palette.

gesting that at the current temporal resolution, recovery time differences are not reliably measurable. This comparison is exploratory: shock resilience was not included in the H1–H8 pre-registration. The shock experiment uses only sparse harshness; extending to other harshness levels would test whether the V3 buffering advantage is consistent across resource regimes and is left as future work.

Effect Size Robustness Check

Exploratory: The alive-count metric used in H1–H8 exhibits ceiling/floor effects in some comparisons ($\delta = 1.00$ with $[1.00, 1.00]$ CI), raising the concern that the metric is too coarse to distinguish strong from overwhelming effects. As a robustness check, we repeat the H1 and H2 comparisons using mean_energy at step 500—a continuous per-entity measure that avoids the binary alive/dead dichotomy. The H1 energy comparison at rich harshness yields $\delta = -0.61$ with CI $[-0.73, -0.47]$—reversed relative to the alive-count direction. V1 entities have higher mean energy (0.432 ± 0.033) than V0 entities (0.402 ± 0.017), indicating that boundary protection benefits individual energy budgets even though population size decreases. The H2 energy comparison at rich yields $\delta = 0.33$ with CI $[0.15, 0.49]$, confirming that V3 benefits are detectable but not saturated on the continuous metric. In medium, sparse, and scarce, both comparisons remain at $\delta = 1.00$. These results demonstrate that the revised model produces a richer range of effect sizes (δ from -0.61 to 1.00) than the prior model's universally saturated values.

Discussion

What the Capability Ladder Tells Us

The phase diagrams (Figure 1) operationalise the virus-to-life transition as a measurable shift in the capability × harshness survival boundary. With the revised model (V1 leakage/damage protection, V2 overconsumption regulation), the ladder reveals environment-dependent tradeoffs rather than a universal cost valley. V1 boundary maintenance shows a genuine cost–benefit tradeoff: it reduces survival in resource-rich environments (where leakage and damage pressure are low relative to repair costs) but provides net protection in harsh environments (where stochastic damage is proportionally more costly). V2 homeostasis mitigates overconsumption waste, providing measurable benefit independent of V3 metabolism (H8). V3 metabolism remains the largest single survival jump, consistent with the biological intuition that internal resource buffering is the key enabling capability. This "cost valley" at V1/V2—followed by V3 recovery—is now shallower and environment-dependent, mirroring the tradeoff structure expected from real virus-to-cell transitions where capsid assembly is costly but provides environmental protection.

Beyond V3, the ladder reveals a second, subtler cost-benefit structure. V4 chemotaxis (H5) improves survival in medium through scarce environments where resource gradients carry useful information (mean alive rises 61–80% over V3) but reduces survival in rich environments (−24%) where uniform abundance makes movement wasteful. V5 lifecycle staging (H6) shows the opposite environment dependence: dormancy and

dispersal pay off only in rich environments (+34% over V4), while in sparse and scarce conditions the dormancy phases suppress replication windows and dispersal's elevated energy cost (×1.5) is counterproductive. These environment-dependent reversals suggest that "more capabilities" is not universally beneficial—each addition is only justified when the environment rewards the specific function it provides. Despite these pairwise reversals, the full V0→V5 trend (H7, JT test) is significant at all harshness levels ($p < 10^{-100}$): the V3 metabolic recovery dominates the aggregate signal.

The H3 ProtoOrganelle liberation result is environment-dependent: in resource-rich conditions, adding V0 replication to a metabolically complete entity (V1+V2+V3) immediately produces a replicating population ($\delta = 1.00$); in sparse/scarce environments, the resource pool is too depleted for the ProtoOrganelle's higher replication threshold (0.80). The liberation contrast is partially self-evident (0 vs. non-0 replications); its value lies in demonstrating that metabolic infrastructure (V1+V2+V3) alone is insufficient without reproductive capability, and that the environment must be sufficiently rich to sustain the higher replication threshold. This suggests that the "liberation" of proto-endosymbionts—gaining independent reproduction—may require not just the right capability but also sufficiently favourable environmental conditions, consistent with serial endosymbiosis scenarios (Maturana and Varela, 1980).

The H4 monotonic trend is significant at all four harshness levels. The Jonckheere-Terpstra test detects an overall upward tendency dominated by the V3 recovery; the non-monotonic intermediate dip means the trend should not be interpreted as strictly monotonic at every step. Rather, the virus-to-life transition is better modelled as a cost-then-benefit trajectory than as a smooth monotonic improvement. The same caveat applies to H7's full V0→V5 trend.

InternalizationIndex as a Life-Likeness Metric

The multi-channel II (Figure 2) addresses a limitation of the single-channel formulation: previously, II was effectively a V3 on/off switch (zero for V0–V2, positive only with V3). The revised four-channel composite rises gradually: V2 activates the regulation channel, V3 the energy channel, V4 the behaviour channel, and V5 the lifecycle channel. Each channel is independently interpretable—II_E measures metabolic self-sufficiency, II_R measures regulatory efficiency, II_B measures behavioural autonomy, and II_L measures lifecycle self-control—enabling validation that the composite is not driven by a single dominant channel. The V3 energy channel remains the largest contributor, consistent with metabolism being the most transformative capability, but V2 and V4 contribute meaningfully. Crucially, the survival benefit of V3 (seen in H2 and Figure 1) is measured from alive counts, not from II, confirming structural independence.

Weak ALife Stance

All claims in this paper are functional analogies. "Boundary maintenance" is functionally analogous to capsid integrity: it provides a per-step cost plus a protective effect that prevents death and blocks premature replication. It does not claim to be a capsid, nor to model capsid biochemistry. The same applies to homeostasis (V2), metabolism (V3), chemotaxis (V4), and staged lifecycle (V5). We take a weak ALife position (Langton, 1989): the computational system models life-like properties without claiming to be alive or to resolve the definition of life.

Limitations

Platform dependence. The background world provides a structured resource landscape and temporal dynamics, but the specific organism population parameters (30 organisms, 25 agents each) influence resource availability patterns. The qualitative findings (cost valley, V3 recovery) are expected to be robust to platform details, but exact effect sizes may shift under different background populations. Future work should validate on alternative resource landscapes (e.g., static gradients, procedurally generated environments).

Scale and duration. The 10-entity initialisation per run and 500-step duration limit population dynamics; for larger-scale phase diagrams, $n_{\text{init}} = 50-100$ and $T = 2000$ would reduce stochastic extinction artefacts. An exploratory robustness analysis at these scales is planned.

Entity interaction. SemiLife entities do not compete with organisms or with each other—the resource field is shared but there is no direct interaction. Introducing competition would add ecological realism (resource depletion effects, niche differentiation) but confounds the clean capability-ladder interpretation; we propose competition as a priority extension.

Future Directions

A competition axis—placing multiple archetypes in the same world simultaneously —would reveal which capability profiles dominate under natural selection. Extending V4 with nonlinear policies (small neural networks) could test whether complex sensing strategies emerge under selection pressure. Allowing V5 stage-transition parameters to evolve would test whether lifecycle timing self-optimises across harshness gradients.

Finally, scaling to larger populations ($n_{\text{init}} = 50{-}100$) and longer runs (>1000 steps) would probe whether the cost valley persists at ecological timescales.

Data Availability

All simulation code, experiment scripts, preregistration, and analysis pipelines are available in the project repository (URL withheld for double-blind review). Raw TSV data files and statistical output (JSON) will be archived on Zenodo upon acceptance, with a persistent DOI linked from the camera-ready manuscript.

References

Anonymous (2026). Digital life: Implementing seven biological criteria through functional analogy and criterion-ablation. In The 2026 Conference on Artificial Life, ALIFE 2026. Submitted; anonymized for double-blind review.

Benner, S. A. (2010). Defining life. Astrobiology, 10(10):1021–1030.

Cleland, C. E. and Chyba, C. F. (2002). Defining 'life'. Origins of Life and Evolution of the Biosphere, 32(4):387–393.

Cliff, N. (1993). Dominance statistics: Ordinal analyses to answer ordinal questions. Psychological Bulletin, 114(3):494–509.

Holm, S. (1979). A simple sequentially rejective multiple test procedure. Scandinavian Journal of Statistics, 6(2):65–70.

Jonckheere, A. R. (1954). A distribution-free k-sample test against ordered alternatives. Biometrika, 41(1–2):133–145.

Langton, C. G. (1989). Artificial Life: Proceedings of an Interdisciplinary Workshop on the Synthesis and Simulation of Living Systems. Addison-Wesley, Redwood City, CA. Reprinted by Routledge, 2019.

Maturana, H. R. and Varela, F. J. (1980). Autopoiesis and Cognition: The Realization of the Living. Boston Studies in the Philosophy and History of Science. Springer Netherlands.

Urry, L. A., Cain, M. L., Wasserman, S. A., Minorsky, P. V., and Reece, J. B. (2020). Campbell Biology. Pearson, New York, 12th edition.